Proton-Exchange Membrane Fuel Cells with Low-Pt Content

Anusorn Kongkanand, Wenbin Gu and Mark F. Mathias
Fuel Cell Business, General Motors Global Propulsion Systems, Pontiac, MI, USA

Article Outline

Glossary

Electrochemically active surface area (ECSA) The surface area of Pt catalyst that is electrochemically active, requiring access to both protons and electrons. It is generally normalized to Pt mass (e.g., m^2/g_{Pt}), and is the primary measure of Pt dispersion.

Fuel cell catalyst Materials that catalyze the electrochemical reactions. Pt or Pt alloy nanoparticles (3–5 nm in diameter) deposited on carbon blacks are commonly used with the goal of maximizing the available reaction site surface area per Pt mass.

Hydrogen PEMFC vehicle Vehicle that uses proton-exchange membrane fuel cell (PEMFC) as its primary power generator, commonly known as fuel cell electric vehicle (FCEV). It uses pure hydrogen gas fuel reacting electrochemically with oxygen gas from the atmosphere to generate electricity and emit only water. Generally requires Pt as electrocatalyst on both anode and cathode.

Ionomer Ion conducting polymer is used in the membrane and electrodes. In PEMFCs, the conducted ion is a proton, and the environment is strongly acidic with effective pH <1. Perfluorosulfonic acid (PFSA) such as Nafion® (DuPont tradename) is the most common.

Local transport loss Performance (i.e., voltage) loss due to the transport of oxygen and protons in close (<30 nm) proximity to the Pt reaction site. Characteristically, this loss is inversely proportional to the Pt roughness factor (i.e., low m^2_{Pt}/m^2_{MEA}) and is most prevalent at high-current density.

Membrane-electrode assembly (MEA) The MEA is at the heart of the fuel cell where the electrochemical reactions occur. Hydrogen oxidation reaction (HOR) occurs in the anode. Oxygen reduction reaction (ORR) occurs in the cathode. The polymer membrane, sandwiched between the two electrodes, conducts proton across from the anode to cathode and acts as an electrical and reactant separator.

Oxygen reduction reaction (ORR) O_2 is electrochemically reduced to water on the cathode. ORR is responsible for most of the overall voltage (i.e., efficiency) loss in a fuel cell even with heavy use of Pt catalyst. Therefore, research on high-activity ORR catalyst is of high priority. ORR kinetic activity is commonly expressed by either normalizing to its Pt mass (mass activity) or to its available Pt surface area (area-specific activity).

PGM Platinum group metals (Pt, Pd, Ir, Ru, Rh, and Os) and other precious metals (Au, Ag, Re) must be minimized or avoided to enable affordable fuel cells.

Pt roughness factor (r.f.) The Pt surface area on an electrode for electrochemical reaction per MEA geometric area (m^2_{Pt}/m^2_{MEA}). This is a product of Pt ECSA (m^2/g_{Pt}) and the MEA Pt loading (g_{Pt}/m^2_{MEA}).

T. E. Lipman, A. Z. Weber (eds.), *Fuel Cells and Hydrogen Production*,
https://doi.org/10.1007/978-1-4939-7789-5_1022

Originally published in
R. A. Meyers (ed.), *Encyclopedia of Sustainability Science and Technology*,

Definition of the Subject

Widespread commercialization of fuel cell electric vehicles (FCEV) relies on further reduction of PGM (platinum group metals) usage. Although enhancements in the activity and stability of the catalyst are necessary, those alone are insufficient. In a fuel cell with low PGM content, transport of reactants (oxygen and protons) to a small area of catalyst can cause large performance loss at high power. Because it is this high-power point that determines the required fuel cell area, these losses drive up the size, and thus the cost, of the fuel cell stack. This entry discusses fuel cell cost reduction with special focus on the challenges and opportunity associated with Pt reduction.

Introduction

PEM fuel cells offer a zero-emission tank-to-wheels solution for sustainable transportation, extending to a well-to-wheels solution when renewable hydrogen is used. Although a few automotive manufacturers, notably Hyundai, Toyota, and Honda, have begun to commercialize fuel cell electric vehicles (FCEV), their high cost limits market penetration. The availability of hydrogen stations is also limited. Yet, major fuel cell developers have defined plausible pathways to reduce the fuel cell vehicle total cost of ownership (vehicle plus fuel cost over life) to approach that of incumbent gasoline-engine vehicles in the long term. Two critical elements of this roadmap include decreasing material cost of the fuel cell system and reducing manufacturing cost through economies of scale.

An automotive fuel cell typically requires about 10 m^2 of electrochemically active area which is distributed over 250–400 individual cells in series, each with 400–250 cm^2 of active area. Each cell is a high-current (>500A) and low-voltage (~0.6 V) device, and cells are stacked in series to deliver high DC power required for vehicle propulsion. The trade-off defining the number of cells and active area is dictated by a cost optimization involving the power electronics that are used to interface the fuel cell stack with the high-voltage electrical system [1], a topic outside of the scope of this entry. Instead, this entry focuses on the issue of reducing overall electrochemically active area needed to produce a given power, an issue that is independent from the trade-off determining the selection of the number of cells.

State-of-the-art FCEVs use about 30 g of Pt [2, 3], the only PGM used in the fuel cell system. At today's (June 2017) Pt price of $30 per gram, the cost of Pt metal itself is about $900, a small fraction of a vehicle cost. But it is significantly larger than what is used in the current clean light-duty internal combustion engine (ICE) vehicle catalytic converter (<5 g PGM, comprising Pt, Pd, and Rh) [4, 5]. Pt is rare, and because of its high resistance to corrosion, it is used in many applications. Of the 218 tons of platinum sold in 2014, 45% was used for vehicle emission control devices, 34% for jewelry, and 9% for chemical production and petroleum refining [6]. The remainder was consumed in other industries including electronics, glass manufacturing, and the medical and biomedical industries. Because Pt is such a well-established commodity, increase in demand will put pressure on its availability and price. Analysis in Fig. 1 shows a significant increase in Pt demand once FCEVs with 10 g_{Pt} penetrate the mass market (scenario B, assumes five million FCEVs/year, about 5% of global vehicle market), generating upward pressure on Pt price [7]. This supply-demand scenario indicates the need for technologies to reduce Pt usage well below 10 g/vehicle in the long run.

Figure 2 illustrates the relationship between cathode Pt loading and the cost of major fuel cell stack components assuming a 2016 state-of-the-art current-voltage curve [2]. Although the Pt cost is a large portion of the stack cost at 0.3 mg_{Pt}/cm^2 (~30 g_{Pt}/vehicle), reducing Pt loading below 0.2–0.1 mg_{Pt}/cm^2 results in only a marginally lower stack cost, and decreasing to 0.05 mg_{Pt}/cm^2 actually results in a stack cost increase. This is due to poor high-power performance of the low-Pt cathode, to be discussed in more detail below, making it necessary to increase stack area and

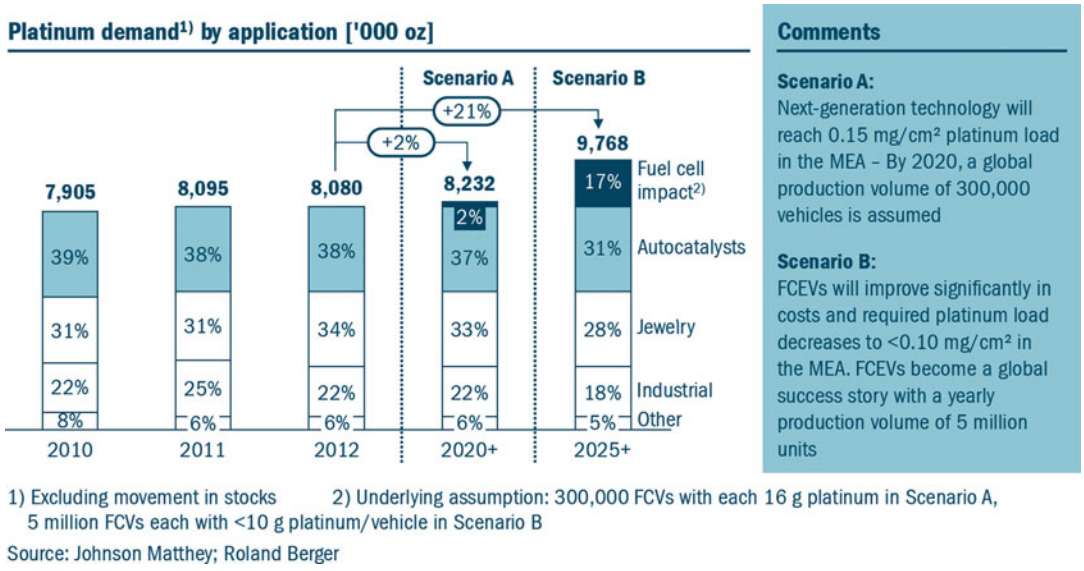

Proton-Exchange Membrane Fuel Cells with Low-Pt Content, Fig. 1 Impact of fuel cell vehicles on Pt consumption (Reprinted with permission from Ref. [7]. Copyright 2013 Roland Berger LLC)

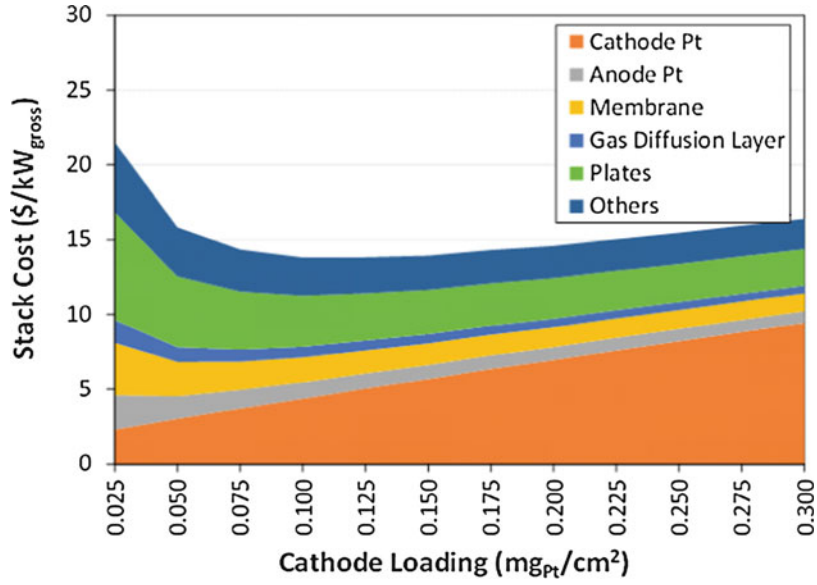

Proton-Exchange Membrane Fuel Cells with Low-Pt Content, Fig. 2 Effect of cathode Pt loading on stack cost. Anode Pt loading is kept constant at 0.025 mg_{Pt}/cm^2. Cost estimated using SA/DOE 2013 cost study, 90 kW_{gross} system, 500 k system/year [8] (Reprinted with permission from Ref. [2] Copyright 2016 American Chemical Society)

overcoming the benefit of the Pt areal-loading decrease. Improvement in the high-power performance of the low-loaded cathode will minimize stack cost and decrease the Pt loading at which the minimum cost occurs. This analysis also indicates that further reduction of Pt loading below 0.1 mg_{Pt}/cm^2 (~10 g_{Pt}/vehicle) must be done with the objective of lowering the overall fuel cell stack cost. Whereas reduction below 0.1 mg_{Pt}/cm^2 with current fuel cell performance may not necessarily be a major vehicle-level cost saver, it would be important to mitigate demand on the global Pt market and thus enable high market penetration of automotive fuel cells.

If 10 g_{Pt}/vehicle could suppress FCEV mass-market penetration due to supply-demand factors, what level is needed to eliminate this barrier? Reductions to a level comparable to the catalytic converter (~5 g PGM/vehicle) would largely neutralize the demand increase due to the corresponding decrease in catalytic converter demand. Thus, 5 g PGM/vehicle is a reasonable long-term target [2]. Other important factors could involve broader PGM market shifts. For example, an average wedding ring weighs about 5 g; thus, many married couples own approximately an FCEV equivalent of Pt. Consider this reference point and the fact that the world is consuming 34% of total Pt consumption for jewelry. Thus, a shift in consumer preference to use Pt to enable emission-free future transportation and to use other metals (tungsten, gold, etc.) for jewelry could have a large beneficial impact on Pt availability and cost for FCEV use.

The ultimate goal of fuel cell catalyst development is to entirely eliminate the need for PGM. Significant progress has been made by packing as many active sites as possible into carbon-nitrogen-based non-PGM catalysts [9–11]. However, their stability is currently unacceptably poor [12]. In addition, their useable power density is only about one-tenth of the PGM catalyst system, making vehicle packaging and cost (e.g., of other stack components that scale with surface area) impractical. Finally, if PGM use is successfully reduced to a level comparable to incumbent vehicle technology (~5 g_{PGM}/vehicle), the economic benefit of an alternative may not be favorable.

Alkaline membrane fuel cells (AMFC) operate under less corrosive conditions, and low-cost non-PGM cathode catalysts may be used [13, 14]. However, palladium is currently still required on the anode to achieve power density, and thus stack size reduction, approaching that possible with PEMFCs. Furthermore, the instability of AMFC membrane candidates at high temperature (80–100 °C) and the deactivation of its ionic carriers due to CO_2 in air are other major technology hurdles [15–17]. These performance, durability, and cost uncertainties have thus far prevented AMFC technology from mounting a serious challenge to PEMFC for automotive applications. AMFC technology status and trajectory is described in detail in a separate entry in this volume.

In this entry, we will provide an overview of the challenges and most promising research directions to develop automotive PEM fuel cell technology with sustainable Pt use.

PEM Fuel Cell Electrodes

The hydrogen oxidation reaction (HOR) on the anode is so fast that less than 1 g of Pt can suffice [18]. And when pure hydrogen is used, fast HOR rate and diffusion minimize the voltage loss on the anode. Therefore, the primary focus has been on improving the sluggish oxygen reduction reaction (ORR) on the cathode. Much progress has been made in improving the activity and stability of the ORR catalysts in the past 15 years. Many advanced catalysts (e.g., shape-/size-controlled alloy [19–24], Pt monolayer catalysts [25–27], etc.) have shown promising activity in rotating disk electrode (RDE) tests, although they have not shown comparable activities in fuel cell membrane-electrode assemblies (MEA). Fortunately, a more gradual improvement using a dealloying approach [28–31] on spherical PtNi and PtCo to control the "Pt skin" and subsurface composition has yielded materials that approach the required activity and stability in a fuel cell for a ~5 g_{Pt}/vehicle [2, 31, 32].

As shown in Fig. 3a, the ORR requires efficient delivery of oxygen, protons, and electrons at the same location. Facile transport of these species, which occur through different phases, to the active site is essential to allow high-power output. The electrodes are generally made of mixtures of proton-conducting polymers (ionomer, blue) and carbon-supported Pt nanoparticle (gray and black circles) catalysts. This design gives a porous layer (~60% porosity) that is good for gas transport and a large active area (roughness factors >30 cm^2_{Pt}/cm^2_{MEA}) for the reaction [33, 34].

Carbon black is the preferred support to disperse Pt-based nanoparticles, thanks to its high electronic conductivity, high surface area for nanoparticle deposition, relatively high stability,

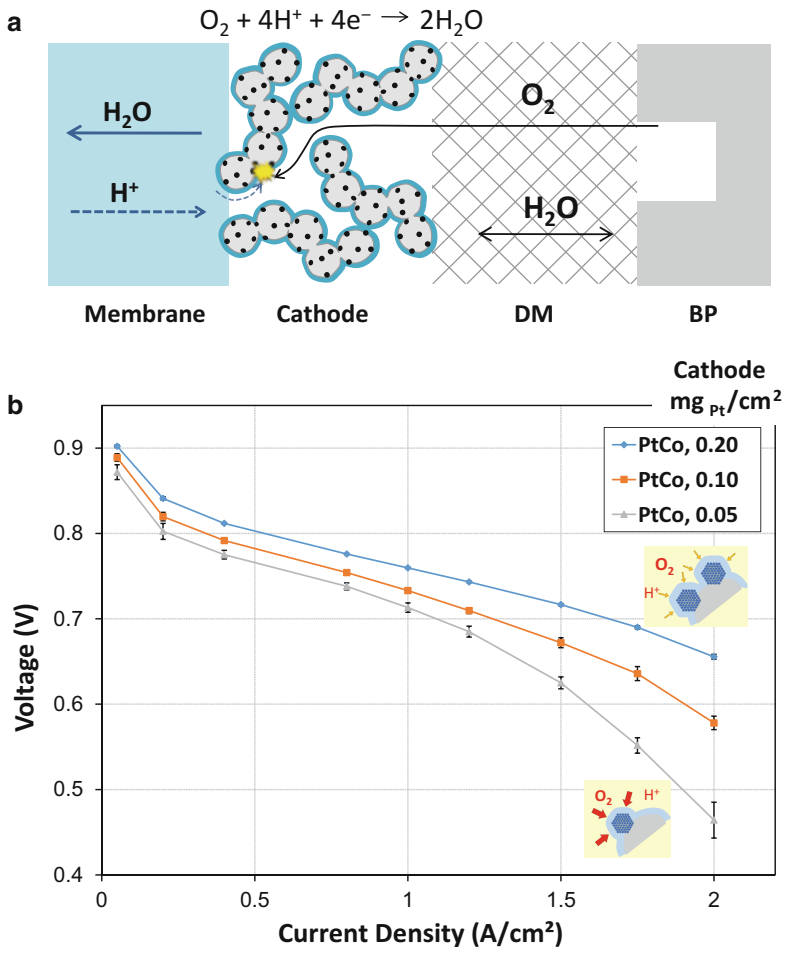

Proton-Exchange Membrane Fuel Cells with Low-Pt Content, Fig. 3 (**a**) Schematic of transport reaction in the fuel cell cathode. (DM = diffusion media; BP = bipolar plate). (**b**) Fuel cell polarization curves of PtCo/C catalyst at different cathode Pt loadings. Operating conditions in the order of anode/cathode: H_2/air, 94 °C, 65/65% RH, 250/250 $kPa_{abs,outlet}$, stoichiometries of 1.5/2. Single cell, 50 cm^2 active area (Reprinted with permission from Ref. [2]. Copyright 2016 American Chemical Society)

and low cost. The morphology and properties of carbon play a critical role in determining the performance and stability of the catalyst [35–39]. Some popular carbons such as KetjenBlack (KB) possess a large number of internal micropores within its carbon particles, making it possible to achieve good Pt particle dispersion and thus high Pt surface area [40, 41]. Figure 4 shows a transmission electron micrograph of a Pt/KB catalyst. Tomography analysis on a section of the catalyst reveals the location of Pt particles in relation to the carbon particle. The red and green coloring represent Pt particles that are located on the surface and within the carbon, respectively.

The presence of the internal Pt adds another set of reactant transport considerations within a fuel cell electrode (Fig. 5). The internal particles have been shown to be mostly electrochemically active and are believed to have access to proton and O_2 through small openings (1–5 nm) in the carbon micropores [40, 41]. But it is believed that the pores are too small for ionomer to intrude and form a direct proton conduction path to the Pt surface [39, 42–45]. Although it is hypothesized that condensed water can conduct protons in these pores, much remains unclear on the exact mechanism and the magnitude of the proton conductivity [46–48]. Additionally, ionomer can form a layer blocking the transport of O_2 and water at the opening leading to increased voltage loss [49, 50]. These complexities may make it appealing to use carbons that do not possess internal porosity. However, it has been shown that porous carbons could offer better Pt dispersion, Pt alloy quality, ORR activity, and catalyst stability [37–39]. Therefore, the best carbon

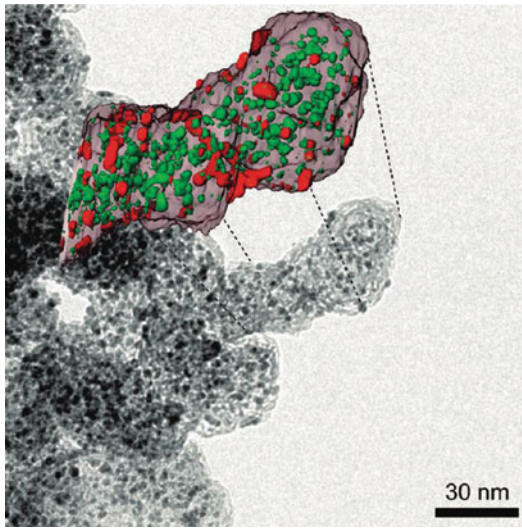

Proton-Exchange Membrane Fuel Cells with Low-Pt Content, Fig. 4 Transmission electron micrograph of Pt nanoparticles deposited on KetjenBlack carbon particles. Color *inset* shows the tomography of an area of the catalyst and the location of Pt particles. *Red* surface Pt. *Green* internal Pt (Reprinted with permission from Ref. [41]. Copyright 2010 American Chemical Society)

support for each user may vary depending on their needs and materials-system trade-off.

Performance of Low-Pt Fuel Cell

At higher power, transport phenomena (oxygen, proton, and electron) in a fuel cell will contribute to the voltage loss. As Pt loading and the available Pt area for ORR are reduced, higher O_2 and proton fluxes must be delivered to the Pt surface which can lead to noticeable and even severe voltage losses. This is particularly noticeable below 0.1 $mg_{Pt}/cm^2{}_{MEA}$ (Fig. 3b), corresponding to <10 g_{Pt}/vehicle. These internal losses in energy within the fuel cell are converted into waste heat which must be removed from the fuel cell using coolant and a radiator. The size of the radiator, and thus the amount of this heat removal, is limited by the frontal area of the vehicle. Depending on system design and requirement, cell voltage at the stack high-power (i.e., rating) point is generally required to be higher than 0.55–0.65 V to allow for waste heat removal from the vehicle and maintain sufficient hydrogen conversion efficiency (>50%) [1, 51]. Assuming that the fuel cell stack is sized at 0.58 V, one can estimate current densities from Fig. 3b of 1.65 and 2.0 A/cm^2 for 0.05 and 0.1 $mgPt/cm^2{}_{MEA}$, respectively. This results in power densities at these points of 0.96 and 1.16 W/cm^2, translating for a 100 kW_{gross} stack to requirements of approximately 10.4 and 8.6 m^2 of fuel cell area, respectively. This case illustrates that although it is in principle desirable to reduce the Pt loading, worse fuel cell performance at the stack rating voltage translates to a 20% increase in overall stack size. Depending on the cost of the fuel cell components that scale with area (e.g., plates, membrane, and diffusion media), this can result in an increase in stack cost even with lower-Pt areal loading, as also shown in Fig. 2 at cathode Pt loadings less than 0.1 mg_{Pt}/cm^2.

A fuel cell performance mathematical model provides a useful tool to help understand the various internal voltage losses. One can build a model using known physics involved in a PEMFC that uses inputs from a number of in situ electrochemical diagnostics and ex situ characterization methods [34, 45]. Figure 6 illustrates the voltage loss terms estimated for various components as a function of current density. While a realistic fuel cell is operated under a wide range of conditions that vary over the fuel cell area, a simplified "differential cell" (i.e., high gas flow and constant temperature condition) is often used, and is modeled here, for diagnostic purposes. By far, ORR kinetic loss is the largest contributor. As current density increases, transport phenomena (oxygen, proton, and electron) contribute to the voltage loss. Ohmic loss (membrane protonic resistance and electronic resistance of other components), O_2 transport loss in the gas diffusion layers, and proton conduction loss in the electrodes are also noticeable. However, these losses do not change with Pt amount and are thus not the focus of this entry. More detail on these losses can be found elsewhere [34, 45].

As Pt loading and its surface area decrease, transport of protons and O_2 to the reaction sites becomes more challenging. Characteristically, this type of loss increases with decreasing Pt

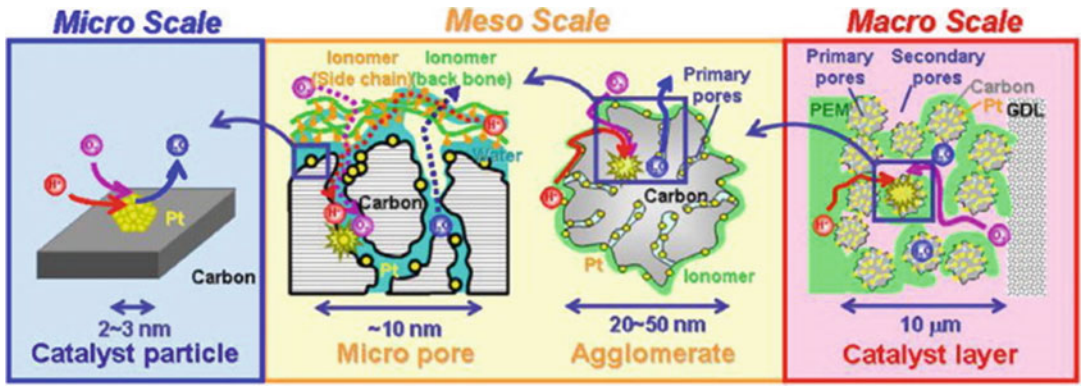

Proton-Exchange Membrane Fuel Cells with Low-Pt Content, Fig. 5 Illustration showing transport of proton, O_2, and water at different length scales in the cathode electrode (Reprinted with permission from Ref. [42]. Copyright 2011 Elsevier)

roughness factor and is called a "local transport loss," postulated to be at or near the Pt surface [52]. As will be discussed in the next section, a portion of this loss can be attributed to the transport of O_2 through an ionomer thin film covering the Pt particle (yellow area). However, there remains voltage loss at high-current density that has not yet been accounted for by known physics or chemistry (orange area). Both losses grow rapidly as current is further increased or as Pt surface area drops further during long-term fuel cell operation. Therefore, they must be understood and minimized for the long-term Pt loading target to be met.

Local Transport Resistance

As discussed in Fig. 6, the local transport resistance can be divided into two components: (a) O_2 transport associated with ionomer thin film (yellow area) and (b) an unaccounted-for resistance (orange area). The latter component is hypothesized to result from proton and O_2 transport through nanometer-sized pores shown in Fig. 5. Some studies constructed "agglomerate" models, simulating impact of 50–500 nm diameter spherical elements filled with water and/or ionomer, in attempts to simulate the voltage loss [45, 49, 50, 53]. Indeed, there are examples indicating that this unaccounted-for loss (orange area) can be largely eliminated when nonporous carbons are used [39, 54–56]. However, due to the complex structural heterogeneity of the electrode (ionomer distribution [57, 58], Pt location [40, 41], carbon pore morphology [42, 44, 59], etc.) as well as engineering phenomena (e.g., localized water generation, drying due to local temperature increase), such models have been difficult to unambiguously test and validate. This area remains in need of improved diagnostics and modeling tools to definitively identify the source of this unaccounted-for loss.

The "O_2 local" component in Fig. 6 can be characterized by a resistance called R_{O2}^{Pt}, and this can be quantified by operating an MEA under O_2 transport-limiting conditions [52, 60]. In this so-called O_2 limiting-current measurement, both the Fickian (pressure-dependent component representing bulk gas transport, R_F) and non-Fickian (pressure-independent component representing Knudsen or through-film transport, R_{NF}) components of the O_2 transport resistance can be determined. Fickian transport represents bulk gas transports in gas-diffusion media and large pores in the microporous layer and electrode. Fickian transport resistance does not change with Pt loading. It is the R_{NF} that strongly correlates with high-current-density (HCD) performance of low-Pt electrodes. Physically, R_{NF} is made up of three transport resistances – one from the small pores in the microporous layer (MPL), another from the small pores in the cathode catalyst layer (CCL), and the third for a region close to the Pt surface [52]:

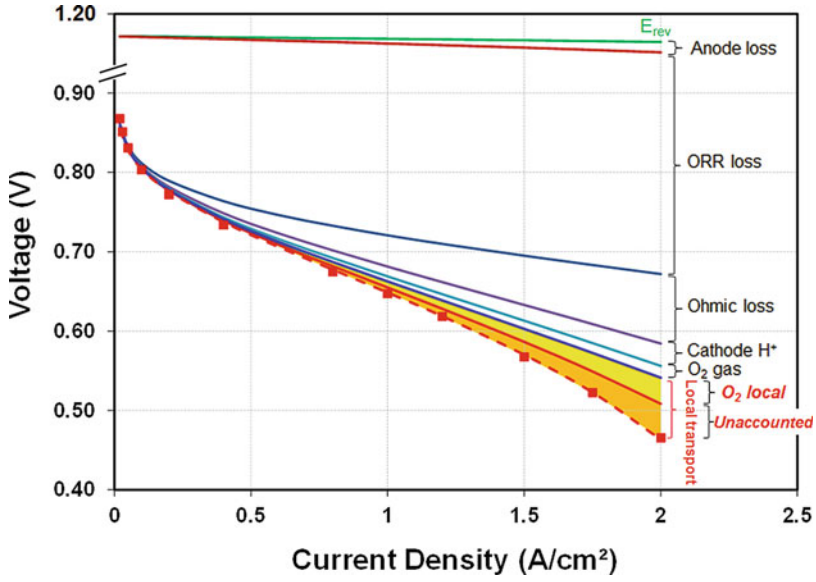

Proton-Exchange Membrane Fuel Cells with Low-Pt Content, Fig. 6 Voltage loss terms in a low-Pt PEMFC operated under differential cell conditions (i.e., high gas flow and constant temperature): H_2/air, 150 kPa_{abs}, 80 °C, and 100% RH. The *symbols* represent the experimental data. The *lines* are the thermodynamic equilibrium cell voltage (E_{rev}) subtracting various voltage losses calculated based on the measured component material and transport properties and electrode kinetics. MEAs: Pt/C anode and Pt/KB cathode (0.025 and 0.056 mg_{Pt}/cm^2, respectively) coated on an 18 μm thick composite membrane

$$R_{\mathrm{NF}} \approx R_{\mathrm{NF}}^{\mathrm{MPL}} + R_{\mathrm{NF}}^{\mathrm{CCL}} + \frac{R_{O2}^{\mathrm{Pt}}}{r.f.} \qquad (1)$$

Figure 7a summarizes the R_{NF} as a function of Pt roughness factor (r.f.) for a variety of cathode catalysts [61]. Electrodes with low r.f. (low Pt loading) show high R_{NF} because more O_2 must be delivered to a smaller Pt surface resulting in a higher apparent electrode O_2 transport resistance. As shown in Eq. 1, one can determine the R_{O2}^{Pt} by plotting R_{NF} vs 1/r.f. (inset). In this case, the R_{O2}^{Pt} is determined to be 11.2 s/cm from the slope. In Fig. 7b, we summarize the fuel cell performance at 1.75 A/cm^2 as a function of roughness factor. The fuel cell voltage drops precipitously once the r.f. is below about 50, as the shrinking available surface area drives up the local reactant flux.

In contrast to the dispersed carbon-supported catalysts discussed above, the 3M nanostructured thin-film (NSTF, blue squares) catalyst shows impressive fuel cell performance despite its very low-Pt r.f. [62–64]. The majority of the 3M NSTF surface is free of ionomer and therefore relies on proton conduction on the Pt surface. However, when a thin (2–4 nm) ionomer film was coated on the NSTF surface, the catalyst exhibited similar behavior to that of the carbon-supported Pt nanoparticle-based (and presumably thin ionomer film coated) catalysts [61, 65, 66].

Ionomer Thin Film and Ionomer-Pt Interface

The above results strongly indicate that ionomer thin film (<5 nm) on the Pt surface contributes to the rise of the "local O_2" resistance (yellow shaded area in Fig. 6). In this section, we discuss potential mechanisms by which the ionomer induces this resistance. Known O_2 permeability of a thick membrane (e.g., a 10–20 μm membrane such as typically used in the fuel cell) cannot explain the large O_2 transport loss observed in the fuel cell electrodes, as there is a factor of 3–10 increase in the apparent resistivity of a thin film [52]. In bulk perfluorosulfonic acid (PFSA)

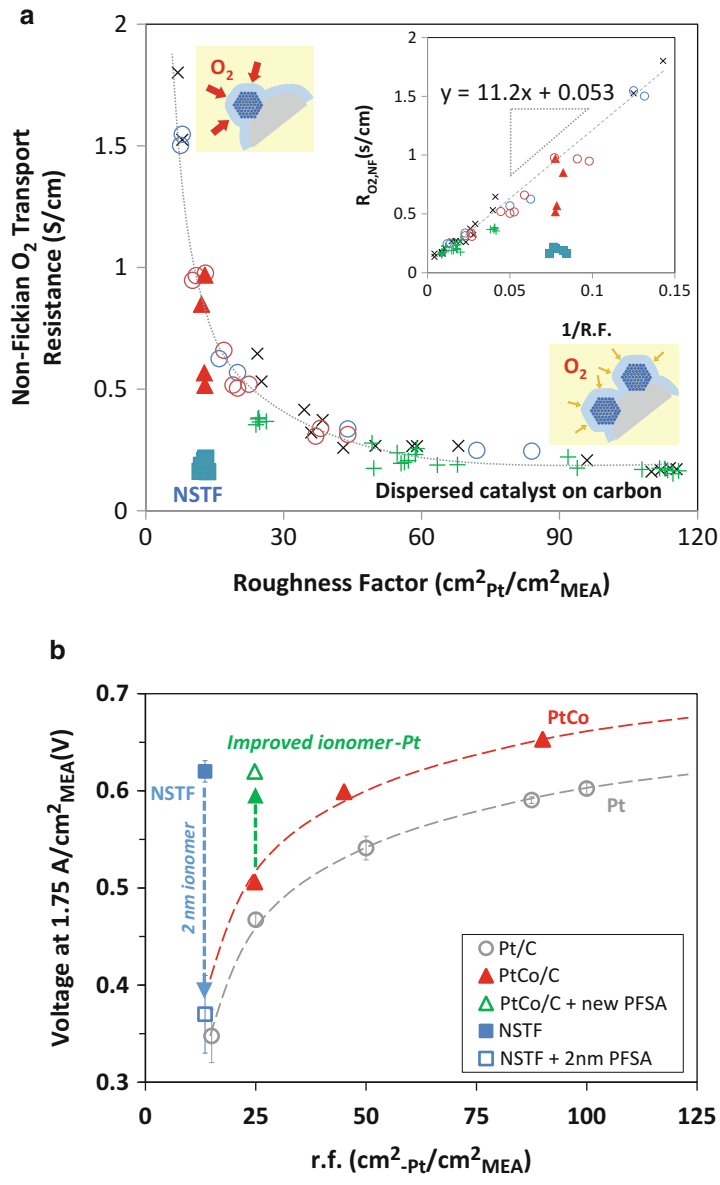

Proton-Exchange Membrane Fuel Cells with Low-Pt Content, Fig. 7 (**a**) Non-Fickian O_2 transport resistance (R_{NF}) as a function of total Pt area on an MEA cathode (roughness factor is defined as the product of Pt loading and ECSA of the catalyst) for different catalysts. Inset is a plot of R_{NF} vs 1/r.f.. Pt/C (×), PtCo/C (○), Pt-ML/Pd/C (+), NSTF (■), NSTF with 2–4 nm ionomer coatings (▲) (Reprinted with permission from Ref. [2]. Copyright 2016 American Chemical Society (**b**) Voltage at 1.75 A/cm^2 showing the impact of r.f. and ionomer)

membrane, the ionomer phase segregates into hydrophobic regions and water-containing domains with 2–5 nm diameter channels. This efficiently segregated two-phase morphology is believed to be an important feature responsible for the superior proton conductivity as well as increased water and O_2 transport rates as compared to non-PFSA membranes [67–69]. In a fuel cell electrode where ionomer exists as a 1–5 nm thin film on Pt and carbon, the dimensions are too small to allow development of the two-phase morphology present in thicker films. The resulting increased importance of interfacial properties and interactions with solid substrates are expected to induce changes in its structure and transport properties (Fig. 8).

When the ionomer film thickness approaches the characteristic domain size of the ionomer, structure and transport properties of the ionomer can change due to the so-called confinement

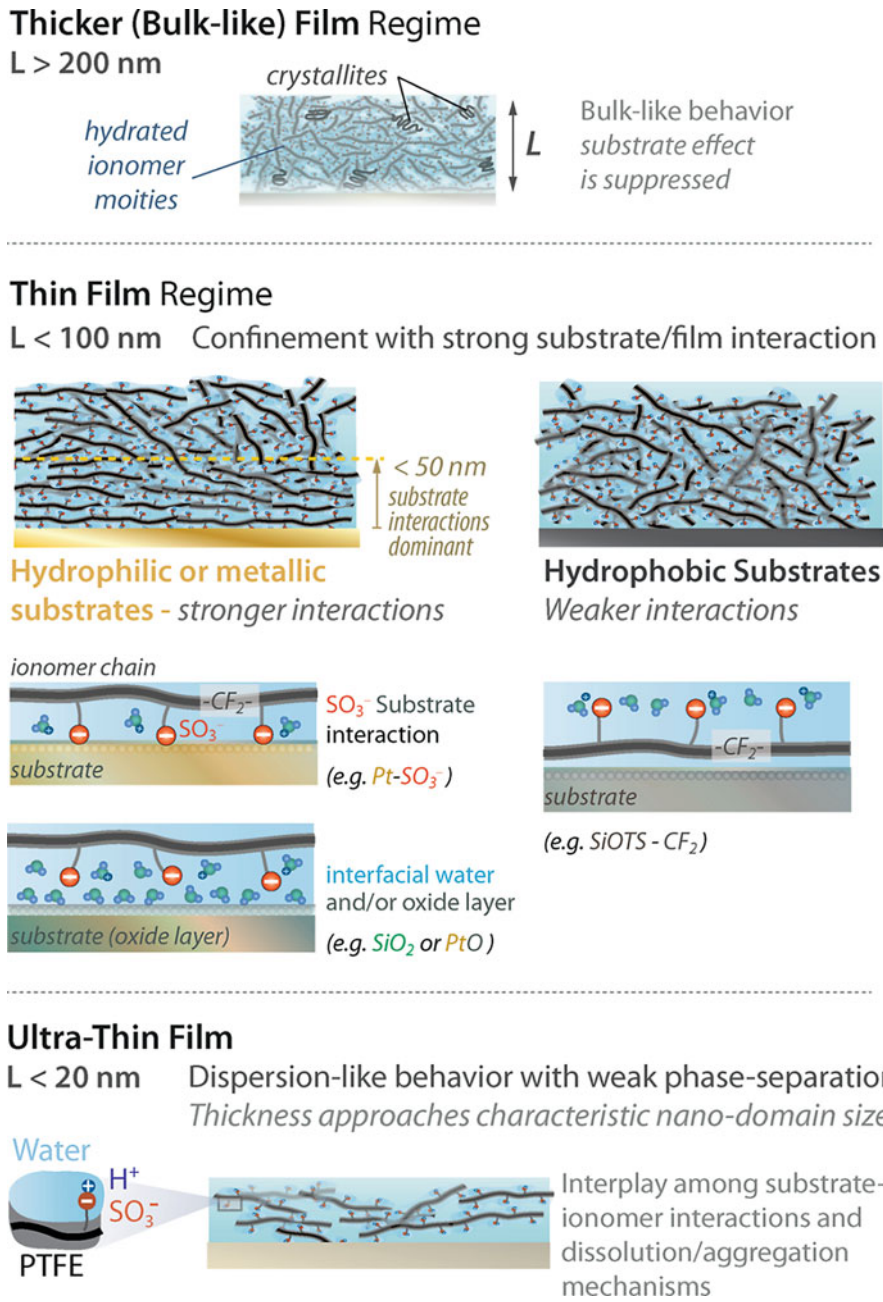

Proton-Exchange Membrane Fuel Cells with Low-Pt Content, Fig. 8 *Thickness* dependence and substrate interaction of ionomer thin film (Reprinted with permission from Ref. [70]. Copyright 2017 American Chemical Society)

effect. Many ex situ techniques such as X-ray scattering, neutron and X-ray reflectivity, TEM, XPS, AFM, and FTIR were employed to study this effect [57, 71–78]. Some effects include a formation of multilamellar nanostructure and reduced transport properties such as lower water uptake and uptake rate [59, 72, 74–77, 79–82]. These effects are highly dependent on treatment condition, substrate type, and operating environments [76, 83]. These findings corroborate

the notion based on domain-size arguments that transport properties of ionomer in a fuel cell electrode are very different from those in bulk membranes. A comprehensive discussion can be found in the PFSA ionomer thin-film entry in this volume and a review by Kusoglu and Weber [70].

Sulfonate groups on the ionomer can adsorb on Pt and reduce ORR activity [84, 85]. The adsorption of the acid group immobilizes the ionomer chain reducing its degrees of freedom [86–88]. Electrodes with higher acid group concentration (lower equivalent weight ionomer) were shown to have higher apparent local O_2 resistance [89]. Some studies showed that different ionomer acid groups and ionic liquid additives can improve ORR activity [24, 90–92]. Furthermore, ex situ O_2 permeability measurement by Litster and coworkers showed that there was no such increase in thin ionomer O_2 resistance when as low as 50 nm thick ionomer films were coated on a polycarbonate substrate and placed in the diffusion path, but not in direct contact with the Pt surface [93]. This result indicates that ionomer interaction with the Pt surface is associated with the increase of the local O_2 resistance.

As an alternative consideration to sulfonate group interaction with Pt, molecular dynamics and DFT simulation by Jinnouchi et al. indicated that it is energetically preferable for the large number of CF_2 groups on the ionomer backbone to fold on the Pt surface [94]. Such a dense layer adjacent to Pt can reduce the O_2 concentration and may be a root cause for the local O_2 resistance.

Published studies using alternative ionomer structures in the electrodes are limited. In general, use of hydrocarbon ionomers results in poor fuel cell performance [95–99]. This is primarily due to their characteristically lower gas permeability which, although favorable when used as a membrane, is detrimental in the electrodes. Among the PFSA ionomers, decrease in the ionomer equivalent weight (increase in the acid group concentration per mass of ionomer) was shown to worsen HCD performance in one study [89]. Ionomers with short side chain or rigid backbone have been shown to mitigate reversible degradation of the electrode [92]. Some acid groups are found to adsorb less strongly to the Pt surface which might translate to higher activity and improved transport properties, although its HCD benefits were not confirmed in actual fuel cell performance [90]. The most significant impact observed is when a small cyclical ring is inserted into the ionomer backbone in order to create a sterically enhanced O_2 permeability through a more open structure (Fig. 9) [100–102]. This results in a substantial improvement in HCD voltage as shown in Fig. 7b (green triangle). These are very encouraging initial results. However, stability and processability concerns still remain.

Altering the process when forming the catalyst layer by changing the solvent system or mixing procedure was shown to improve HCD performance [103–105]. However, it is uncertain whether these enhancements are due to local transport (characteristically scales with Pt

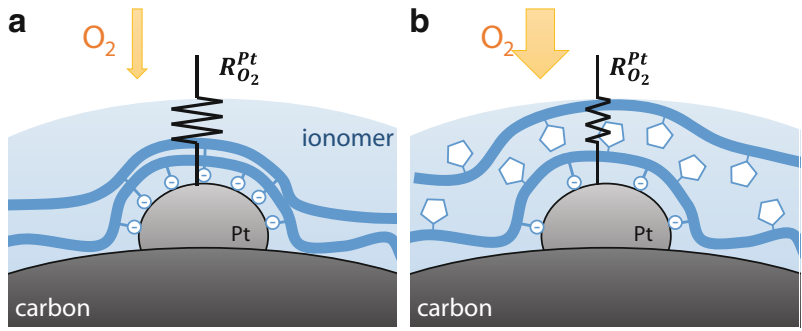

Proton-Exchange Membrane Fuel Cells with Low-Pt Content, Fig. 9 Schematics of hypothesized ionomer structure at the Pt surface for conventional ionomer (**a**) and high-oxygen-permeable ionomer (**b**) (Reprinted with permission from Ref. [2]. Copyright 2016 American Chemical Society)

loading) or optimization of ionomer distribution in the electrode.

Recent studies on ionomer thin films have identified many changes in the microstructure and physical properties of the ionomer; however, large gaps still remain in understanding how these changes affect its transport properties (oxygen, proton, and water) within the cathode as well as how the ionomer structure might change with operating conditions in a fuel cell. These topics are critical future research areas that could have significant positive impact on cathode performance and durability.

Catalyst Roadmap

The mathematical model discussed above can also be used to create catalyst roadmaps that consider the impact of the local transport resistance, indicating critical ex situ measured parameter requirements needed to achieve performance targets. Figure 10 shows catalyst requirements, ORR mass activity, and Pt surface area (ECSA), needed for acceptable performance (>0.58 V) at 1.5 and 2.0 A/cm^2 for cathode catalyst loadings of 0.05 and 0.1 mg$_{Pt}$/cm^2. Requirements with (parabolic dashed lines) and without the local resistance (horizontal dotted lines) are shown. Parameters must be higher than the dashed parabolic lines in order to meet the associated requirement, and materials with values in the upper right-hand portion of the plot are most desirable. Some experimental data are also shown on the map – open symbols are representative MEA data before and after durability tests for four well-known catalyst families. The arrows show significant deleterious impact of degradation during operation, representing a large opportunity if catalyst behavior could be stabilized close to beginning-of-life

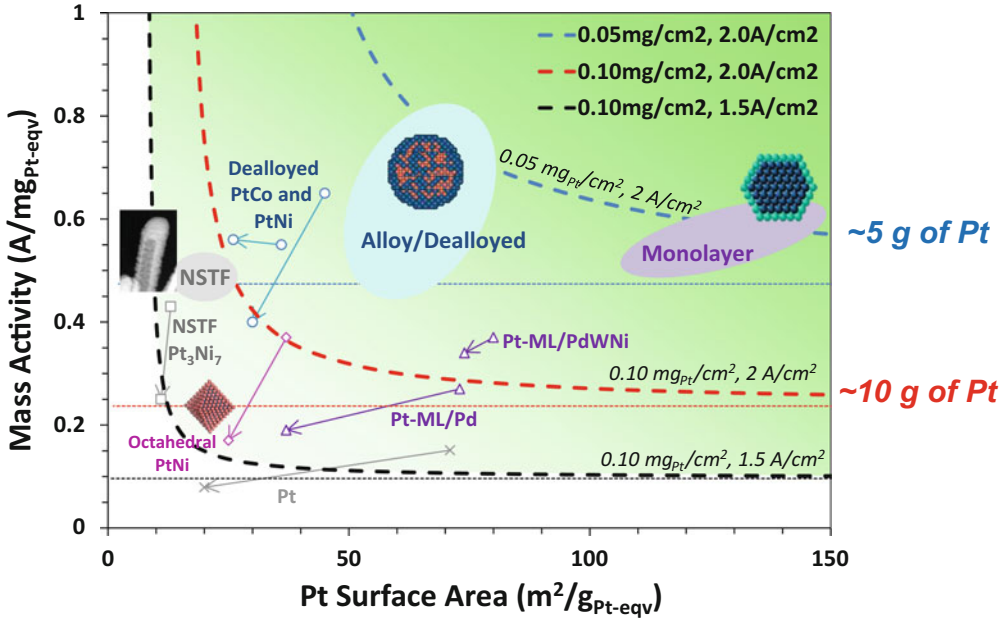

Proton-Exchange Membrane Fuel Cells with Low-Pt Content, Fig. 10 ORR mass activity and Pt ECSA targets which enable the cathode to meet vehicle requirements (0.58 V) at the indicated current density and cathode catalyst loadings. Local resistance of 12 s/cm was used in the analysis. *Dashed lines* and *dotted lines* show the minimum values to meet the requirement with and without local resistance, respectively. Catalysts that are above and to the right of a given boundary are sufficient to meet or exceed the voltage requirement. Data points from MEAs before (*arrow start*) and after (*arrow end*) accelerated durability tests are shown for various catalyst systems [31, 106, 107], and shaded areas indicate estimate of achievable targets (Reprinted with permission from Ref. [2]. Copyright 2016 American Chemical Society)

values. The shaded ovals represent an optimistic expectation of what each approach may achieve in the next 10 years.

Pt alloy catalysts are the most mature. The Toyota Mirai FCEV, introduced to the market in 2014, already uses this type of catalyst although at a higher Pt loading [3, 108]. The high ORR mass activity and moderate Pt surface area suggest that the current catalysts can meet requirement at 10 g_{Pt}/vehicle (red dashed line) but fall short of 5 g_{Pt}/vehicle (blue-dashed line) [31, 32]. Increase in both ORR activity and Pt surface area over operating life is required. Other promising advanced catalysts (e.g., shape-/size-controlled alloy [19–24], Pt monolayer catalysts [25–27], etc.) have shown some encouraging initial results but have generally not yet shown competitive stability in fuel cell MEA testing. Furthermore, they are still made in small quantities at lab scale, and processes amenable to high-volume production remain to be developed.

The Pt monolayer catalyst family pioneered by Brookhaven National Laboratory, shown toward the upper right-hand portion of Fig. 10, is conceptually appealing in that it places essentially all Pt atoms on the particle surface and does not waste Pt atoms in the particle core [25, 26]. This construction gives the highest Pt surface area possible, and representative data are shown in Fig. 11. On a Pt content basis, this catalyst outperforms other types of catalyst, thanks to its high Pt ECSA [27]. However, at the current stage, a relatively large amount of Pd is needed to form Pt monolayer shell, and Pd is subject to leaching out from the core resulting in destabilization of the Pt monolayer [26, 27, 109]. Furthermore, global tightening of automotive emissions standards has raised the price of Pd in recent years to the point that economical advantage of Pd over Pt is minimal. (Both are about $30/g in June 2017.) Some early work on platinum-monolayer shell on palladium-tungsten-nickel core catalyst (Pt-ML/PdWNi), in which half the Pd core has been replaced by less expensive materials, has shown promising performance and durability (middle of Fig. 10). Further work along these lines, pursuing reduction of Pd use and stabilization of the core materials, appears to be a worthwhile development direction.

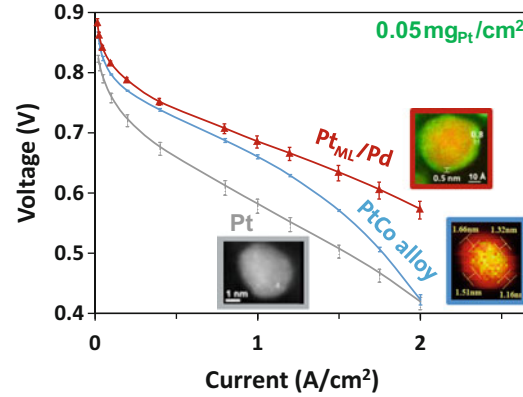

Proton-Exchange Membrane Fuel Cells with Low-Pt Content, Fig. 11 H_2/air polarization curves of different catalysts with Pt loadings of 0.05 mg$_{Pt}$/cm^2. Pt$_{ML}$/Pd catalyst contains 15 wt% Pt and 25 wt% Pd (Reprinted with permission from Ref. [27]. Copyright 2016 American Chemical Society)

Durability of Low-Pt Fuel Cell

Usable performance of the fuel cell must extend over the lifetime of the vehicle (>12 years). Automotive producers generally aim to allow less than 10–20% performance degradation over its life. In the context of Fig. 10, one will need at the end of expected life a catalyst that remains higher than the required ORR activity and Pt ECSA. Characteristics of the degradation of the catalyst and electrode can be observed through decrease in ORR activity and Pt ECSA and loss of transport properties. These losses can be either permanent or reversible. The major degradation mechanisms include Pt and transition metal dissolution, particle migration and coalescence, carbon corrosion, and contaminant adsorption. An extensive review of this topic is available in Ref. [110].

Although one might expect the degradation of a catalyst to be relatively independent of Pt loading, more systematic study is warranted. And even if degradation mechanisms and rates in a low-Pt electrode are the same as in a higher-Pt electrode, the impact on voltage loss will be higher in the low-Pt case. This is because, as discussed in Figs. 7b and 10, the voltage drops precipitously at low r.f. since the resistance (and thus loss) is inversely proportional to this factor. Therefore, research to develop and implement low-Pt

catalysts that start and end life with high ECSA and specific activity is critical to the pursuit of affordable automotive fuel cells.

As the total Pt surface area is reduced in a low-Pt fuel cell, the electrodes become more susceptible to contamination. Some chemical degradation is reversible, and performance can be recovered during normal vehicle operating modes. On the anode, H_2 fuel quality is critical to allow Pt reduction (<0.025 mg_{Pt}/cm^2), where contaminants such as CO and H_2S must be carefully controlled. On the cathode side, a chemical air filter may be required to remove potential contaminants (SO_x, H_2S, NO_x, volatile organic compounds, etc.) from intake air [111, 112]. In addition to external contaminants, degradation products (sulfate and organic compounds from the membrane [66, 113–115]; cobalt from the catalyst [116, 117]) from within the fuel cell MEA can also decrease fuel cell cathode performance. Development of more stable MEA components and strategies to mitigate degradation are needed to enable low-Pt fuel cells under real-world application.

Other Challenges

In this entry, we have focused on the performance of the catalyst and cathode electrode. However, for further improvement other components in the fuel cell must also be developed. Figure 12 breaks down the sources of the voltage loss at high-current density for the near-term target of 0.1 mg_{Pt}/cm^2 at 2 A/cm^2 (upper left, about 10 g_{Pt}/vehicle) and possible paths toward further improvement. For further Pt and cost reduction, one can reduce the Pt loading or increase the maximum current density. To decrease Pt loading (mg_{Pt}/cm^2) at the same current density (move to right in Fig. 12), improvement in ORR activity and local transport are key enablers. To increase current density at the same Pt loading

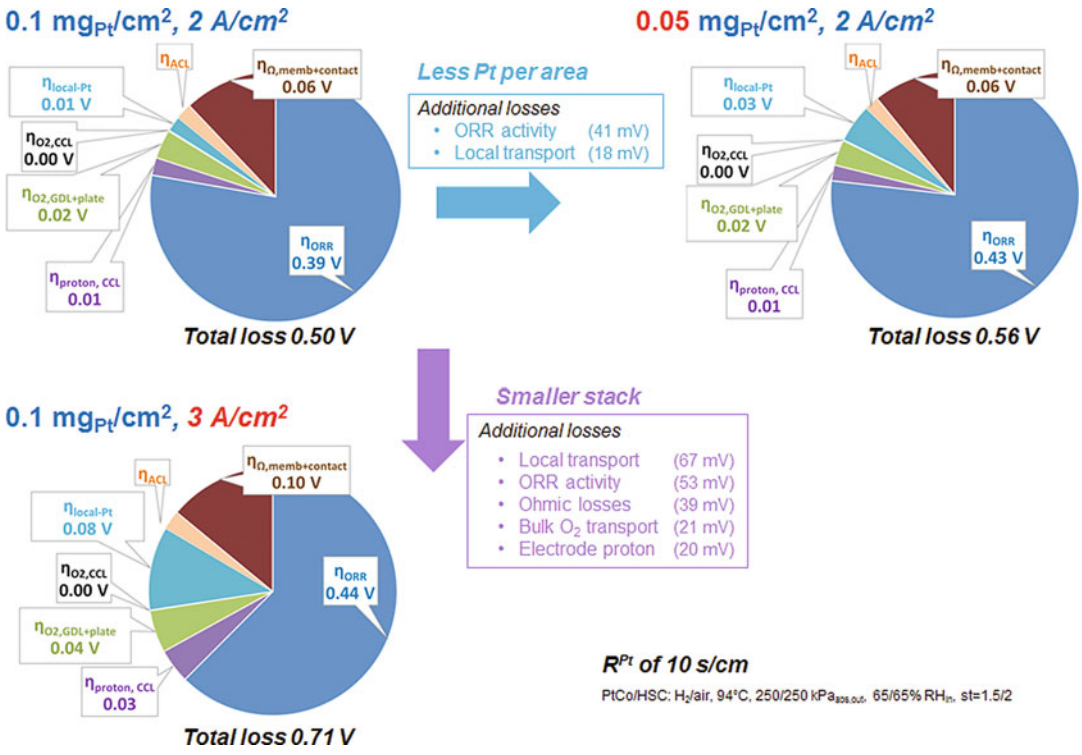

Proton-Exchange Membrane Fuel Cells with Low-Pt Content, Fig. 12 Two pathways to reducing cost further [1]: decreasing Pt loading and [2] increasing current density. Losses are estimated using a fuel cell voltage loss model

(move downward in Fig. 12), improvement in ORR activity and local transport remain of highest priority, but important issues broaden to include ohmic loss reduction, bulk O_2 transport, and cathode proton conduction in the cathode. This downward path can have higher cost reduction impact since smaller stack size will also reduce the amount of bipolar plate, membrane, electrode, and diffusion media material required.

Finally, in order to realize a truly sustainable technology, more precious metals must be recycled. Although growing in recently years, recycling currently only accounts for 30% of the global PGM supply [6]. Pt global recycling rates (60–70%) are better than those of other PGMs thanks to its favorable recycling economics. However, in the automotive sector, the recycling rate only reaches 50–55% [118]. Recycling of PGM is not only technically feasible and environmental friendly but also profitable. Recycling rates can be increased through improved waste collection mechanisms, as well as shifting public perspective from "waste management" to "resource management" [119]. Management of PGM life cycle ultimately needs to expand across many markets and applications including automotive, jewelry, and electronics. For this to occur, strong support will likely be needed from policy makers at state, federal, and international levels.

Future Directions

Fuel cell electric vehicles with about 30 g of Pt are now on the road [2, 3], and next-generation FCEVs are expected to use about 10–25 g of PGM. These are significant accomplishments and encouraging progress toward commercializing this sustainable transportation technology. However, considering commercial factors as well as promising catalyst technologies early in the pipeline, a long-term PGM target is warranted at a level comparable to that used in automotive catalytic convertors (~5 g_{PGM}). Progress in Pt-based catalysts in recent years has been due to alloy optimization resulting in notable activity gains, but opportunities remain to achieve better Pt surface area (ECSA) and alloy stability over operating life. In addition to these structure and kinetics considerations, fundamental understanding of the origin of the local transport resistance is needed in order to optimally engineer the nanostructure near the catalyst active surfaces. Development of ionomer specifically designed for this purpose is a promising research direction, as encouraging early data exists. New issues will be encountered as the use of low-Pt roughness factor increases contamination susceptibility, and fundamental studies to conclusively identify poisoning mechanisms and mitigations approaches will also be needed. Judging from the steady progress made in the past decades, we are optimistic that the concerted efforts of materials developers and electrode designers can resolve these issues, enabling fuel cell vehicles that are affordable for the mass market.

Acknowledgments This work was partially supported by the US Department of Energy, Office of Energy Efficiency and Renewable Energy under grant DE-EE0007271.

Bibliography

Primary Literature

1. Masten DA, Bosco AD (2010) System design for vehicle applications: GM/Opel. In: Handbook of fuel cells. Wiley, Hoboken
2. Kongkanand A, Mathias MF (2016) The priority and challenge of high-power performance of low-platinum proton-exchange membrane fuel cells. J Phys Chem Lett 7(7):1127–1137
3. Gröger O, Gasteiger HA, Suchsland J-P (2015) Review – electromobility: batteries or fuel cells? J Electrochem Soc 162(14):A2605–A2622
4. Fornalczyk A, Saternus M (2009) Removal of platinum group metals from the used auto catalytic converter. Metalurgija 48(2):133–136
5. Nguyen T., Andress D.; Howden, K.; Toops, T., Das S (n.d.) Platinum Group Metals (PGM) for light-duty vehicles. https://www.hydrogen.energy.gov/pdfs/16006_pgm_light_duty_vehicles.pdf
6. Loferski PJ (2014) Minerals yearbook; Platinum-Group Metals. http://minerals.usgs.gov/minerals/pubs/commodity/platinum/myb1-2014-plati.pdf
7. Bernhart W, Riederle S, Yoon M (n.d.) Fuel cells – a realistic alternative for zero emission? https://www.rolandberger.com/en/Publications/pub_fuel_cells_a_realistic_alternative_for_zero_emission.html
8. James BD, Moton JM, Colella WG (n.d.) Mass production cost estimation of direct H2 PEM fuel cell systems

for transportation applications: 2013 update. Strategic Analysis, Inc. http://energy.gov/sites/prod/files/2014/11/f19/fcto_sa_2013_pemfc_transportation_cost_analysis.pdf
9. Proietti E, Jaouen F, Lefèvre M, Larouche N, Tian J, Herranz J, Dodelet J-P (2011) Iron-based cathode catalyst with enhanced power density in polymer electrolyte membrane fuel cells. Nat Commun 2:416
10. Wu G, More KL, Johnston CM, Zelenay P (2011) High-performance electrocatalysts for oxygen reduction derived from polyaniline, iron, and cobalt. Science 332(6028):443–447
11. Jaouen F, Proietti E, Lefèvre M, Chenitz R, Dodelet J-P, Wu G, Chung HT, Johnston CM, Zelenay P (2011) Recent advances in non-precious metal catalysis for oxygen-reduction reaction in polymer electrolyte fuel cells. Energy Environ Sci 4(1):114
12. Banham D, Ye S, Pei K, Ozaki J-I, Kishimoto T, Imashiro Y (2015) A review of the stability and durability of non-precious metal catalysts for the oxygen reduction reaction in proton exchange membrane fuel cells. J Power Sources 285:334
13. Varcoe JR, Slade RCT (2005) Prospects for alkaline anion-exchange membranes in low temperature fuel cells. Fuel Cells 5(2):187–200
14. Merle G, Wessling M, Nijmeijer K (2011) Anion exchange membranes for alkaline fuel cells: a review. J Membr Sci 377(1–2):1–35
15. Yanagi H, Fukuta K (2008) Anion exchange membrane and ionomer for alkaline membrane fuel cells (AMFCs). ECS Trans 16:257–262
16. Einsla BR, Chempath S, Pratt LR, Boncella JM, Rau J, Macomber C, Pivovar BS (2007) Stability of cations for anion exchange membrane fuel cells. ECS Trans 11:1173–1180
17. Pan J, Lu S, Li Y, Huang A, Zhuang L, Lu J (2010) High-performance alkaline polymer electrolyte for fuel cell applications. Adv Funct Mater 20(2):312–319
18. Neyerlin KC, Gu W, Jorne J, Gasteiger HA (2007) Study of the exchange current density for the hydrogen oxidation and evolution reactions. J Electrochem Soc 154(7):B631
19. Zhang J, Yang H, Fang J, Zou S (2010) Synthesis and oxygen reduction activity of shape-controlled Pt(3)Ni nanopolyhedra. Nano Lett 10(2):638–644
20. Wu J, Zhang J, Peng Z, Yang S, Wagner FT, Yang H (2010) Truncated octahedral Pt3Ni oxygen reduction reaction electrocatalysts. J Am Chem Soc 132(14):4984–4985
21. Carpenter MK, Moylan TE, Kukreja RS, Atwan MH, Tessema MM (2012) Solvothermal synthesis of platinum alloy nanoparticles for oxygen reduction electrocatalysis. J Am Chem Soc 134(20):8535–8542
22. Choi SI, Xie S, Shao M, Odell JH, Lu N, Peng H-C, Protsailo L, Guerrero S, Park J, Xia X, Wang J, Kim MJ, Xia Y (2013) Synthesis and characterization of 9 Nm Pt – Ni octahedra with a record high activity of 3.3 A/mg. Nano Lett 13:3420–3425
23. Gan L, Cui C, Heggen M, Dionigi F, Rudi S, Strasser P (2014) Element-specific anisotropic growth of shaped platinum alloy nanocrystals. Science 346(6216):1502–1506
24. Chen C, Kang Y, Huo Z, Zhu Z, Huang W, Xin HL, Snyder JD, Li D, Herron JA, Mavrikakis M, Chi M, More KL, Li Y, Markovic NM, Somorjai GA, Yang P, Stamenkovic VR (2014) Highly crystalline multimetallic nanoframes with three-dimensional electrocatalytic surfaces. Science 343(6177):1339–1343
25. Zhang J, Mo Y, Vukmirovic MB, Klie R, Sasaki K, Adzic RR (2004) Platinum monolayer electrocatalysts for O2 reduction: Pt monolayer on Pd(111) and on carbon-supported Pd nanoparticles. J Phys Chem B 108(30):10955–10964
26. Sasaki K, Naohara H, Cai Y, Choi YM, Liu P, Vukmirovic MB, Wang JX, Adzic RR (2010) Core-protected platinum monolayer shell high-stability electrocatalysts for fuel-cell cathodes. Angew Chemie Int Ed 49(46):8602–8607
27. Kongkanand A, Subramanian NP, Yu Y, Liu Z, Igarashi H, Muller DA (2016) Achieving high-power PEM fuel cell performance with an ultralow-Pt-content core–shell catalyst. ACS Catal 6(3):1578–1583
28. Oezaslan M, Heggen M, Strasser P (2012) Size-dependent morphology of dealloyed bimetallic catalysts: linking the nano to the macro scale. J Am Chem Soc 134(1):514–524
29. Jia Q, Caldwell K, Ziegelbauer JM, Kongkanand A, Wagner FT, Mukerjee S, Ramaker DE (2014) The role of OOH binding site and Pt surface structure on ORR activities. J Electrochem Soc 161(14):F1323–F1329
30. Caldwell KM, Ramaker DE, Jia Q, Mukerjee S, Ziegelbauer JM, Kukreja RS, Kongkanand A (2015) Spectroscopic in situ measurements of the relative Pt skin thicknesses and porosities of dealloyed PtMn (Ni, Co) electrocatalysts. J Phys Chem C 119(1):757–765
31. Han B, Carlton CE, Kongkanand A, Kukreja RS, Theobald BR, Gan L, O'Malley R, Strasser P, Wagner FT, Shao-Horn Y (2015) Record activity and stability of dealloyed bimetallic catalysts for proton exchange membrane fuel cells. Energy Environ Sci 8(1):258–266
32. Kongkanand A (n.d.) DOE final report: high-activity dealloyed catalysts. http://www.osti.gov/scitech/servlets/purl/1262711
33. Gasteiger HA, Kocha SS, Sompalli B, Wagner FT (2005) Activity benchmarks and requirements for Pt, Pt-alloy, and non-Pt oxygen reduction catalysts for PEMFCs. Appl Catal B Environ 56(1–2):9–35
34. Gu W, Baker DR, Liu Y, Gasteiger HA (2009) Proton exchange membrane fuel cell (PEMFC) down-the-channel performance model. In: Vielstich W, Gasteiger HA, Lamm A, Yokokawa H (eds) Handbook of fuel cells: fundamentals, technology and applications. Wiley, Hoboken
35. Antolini E (2009) Carbon supports for low-temperature fuel cell catalysts. Appl Catal B Environ 88(1–2):1–24

36. Yu PT, Gu W, Makharia R, Wagner FT, Gasteiger HA (2006) The impact of carbon stability on PEM fuel cell startup and shutdown voltage degradation. ECS Trans 3:797–809
37. Tuaev X, Rudi S, Strasser P (2016) The impact of the morphology of the carbon support on the activity and stability of nanoparticle fuel cell catalysts. Cat Sci Technol 6(23):8276–8288
38. Park YC, Tokiwa H, Kakinuma K, Watanabe M, Uchida M (2016) Effects of carbon supports on Pt distribution, ionomer coverage and cathode performance for polymer electrolyte fuel cells. J Power Sources 315:179–191
39. Kongkanand A, Yarlagadda V, Garrick T, Moylan TE, Gu W (2016) Electrochemical diagnostics and modeling in developing the PEMFC cathode. ECS Trans 75(14):25
40. Ito T, Matsuwaki U, Otsuka Y, Hatta M, Hayakawa K, Matsutani K, Tada T, Jinnai H (2011) Three-dimensional spatial distributions of Pt catalyst nanoparticles on carbon substrates in polymer electrolyte fuel cells. Electrochemistry 79(5):374–376
41. Jinnai H, Spontak RJ, Nishi T (2010) Transmission electron microtomography and polymer nanostructures. Macromolecules 43(4):1675
42. Ohma A, Mashio T, Sato K, Iden H, Ono Y, Sakai K, Akizuki K, Takaichi S, Shinohara K (2011) Analysis of proton exchange membrane fuel cell catalyst layers for reduction of platinum loading at Nissan. Electrochim Acta 56(28):10832–10841
43. Iden H, Mashio T, Ohma A (2013) Gas transport inside and outside carbon supports of catalyst layers for PEM fuel cells. J Electroanal Chem 708:87–94
44. Shinozaki K, Yamada H, Morimoto Y (2011) Relative humidity dependence of Pt utilization in polymer electrolyte fuel cell electrodes: effects of electrode thickness, ionomer-to-carbon ratio, ionomer equivalent weight, and carbon support. J Electrochem Soc 158(5):B467
45. Weber AZ, Borup RL, Darling RM, Das PK, Dursch TJ, Gu W, Harvey D, Kusoglu A, Litster S, Mench MM, Mukundan R, Owejan JP, Pharoah JG, Secanell M, Zenyuk IV (2014) A critical review of modeling transport phenomena in polymer-electrolyte fuel cells. J Electrochem Soc 161(12):F1254–F1299
46. Zenyuk IV, Litster S (2012) Spatially resolved modeling of electric double layers and surface chemistry for the hydrogen oxidation reaction in water-filled platinum-carbon electrodes. J Phys Chem C 116(18): 9862–9875
47. Zenyuk IV, Litster S (2014) Modeling ion conduction and electrochemical reactions in water films on thin-film metal electrodes with application to low temperature fuel cells. Electrochim Acta 146:194–206
48. Nouri-Khorasani A, Malek K, Malek A, Mashio T, Wilkinson DP, Eikerling MH (2016) Molecular modeling of the proton density distribution in a water-filled slab-like nanopore bounded by Pt oxide and ionomer. Catal Today 262:133–140
49. Nonoyama N, Okazaki S, Weber AZ, Ikogi Y, Yoshida T (2011) Analysis of oxygen-transport diffusion resistance in proton-exchange-membrane fuel cells. J Electrochem Soc 158(4):B416
50. Sadeghi E, Eikerling M, Putz A (2013) Hierarchical model of reaction rate distributions and effectiveness factors in catalyst layers of polymer electrolyte fuel cells. J Electrochem Soc 160(10):F1159–F1169
51. Ahluwalia RK, Wang X, Steinbach AJ (2016) Performance of advanced automotive fuel cell systems with heat rejection constraint. J Power Sources 309:178
52. Greszler TA, Caulk D, Sinha P (2012) The impact of platinum loading on oxygen transport resistance. J Electrochem Soc 159(12):F831–F840
53. Epting WK, Litster S (2012) Effects of an agglomerate size distribution on the PEFC agglomerate model. Int J Hydrog Energy 37(10):8505–8511
54. Murata S, Imanishi M, Hasegawa S, Namba R (2014) Vertically aligned carbon nanotube electrodes for high current density operating proton exchange membrane fuel cells. J Power Sources 253:104–113
55. Kongkanand A (2017) Highly accessible catalysts for durable high-power performance. Annual merit review DOE hydrogen and fuel cells and vehicle technologies programs. Washington, DC. https://www.hydrogen.energy.gov/pdfs/review17/fc144_kongkanand_2017_o.pdf
56. Neyerlin KC, Christ JM, Zack JW, Gu W, Kumaraguru S, Kongkanand A, Kocha SS (2016) New insights from electrochemical diagnostics pertaining to the high current density performance of Pt-based catalysts. Meet Abstr MA2016-02(38):2492
57. Lopez-Haro M, Guétaz L, Printemps T, Morin A, Escribano S, Jouneau P-H, Bayle-Guillemaud P, Chandezon F, Gebel G (2014) Three-dimensional analysis of Nafion layers in fuel cell electrodes. Nat Commun 5:5229
58. Cullen DA, Koestner R, Kukreja RS, Liu ZY, Minko S, Trotsenko O, Tokarev A, Guetaz L, Meyer HM, Parish CM, More KL (2014) Imaging and microanalysis of thin ionomer layers by scanning transmission electron microscopy. J Electrochem Soc 161(10): F1111–F1117
59. Iden H, Sato K, Ohma A, Shinohara K (2011) Relationship among microstructure, ionomer property and proton transport in pseudo catalyst layers. J Electrochem Soc 158(8):B987
60. Baker DR, Caulk DA, Neyerlin KC, Murphy MW (2009) Measurement of oxygen transport resistance in PEM fuel cells by limiting current methods. J Electrochem Soc 156(9):B991
61. Makharia R (2010) Challenges associated with high current density performance of low Pt-loading cathodes in proton exchange membrane (PEM) fuel cells. In: ASME 8th international fuel cell science, engineering & technology conference, Brooklyn, 2010
62. Debe MK (2012) Effect of electrode surface area distribution on high current density performance of PEM fuel cells. J Electrochem Soc 159(1):B54

63. Sinha PK, Gu W, Kongkanand A, Thompson E (2011) Performance of nano structured thin film (NSTF) electrodes under partially-humidified conditions. J Electrochem Soc 158(7):B831
64. Debe MK (2012) Electrocatalyst approaches and challenges for automotive fuel cells. Nature 486(7401):43–51
65. Kongkanand A, Owejan JE, Moose S, Dioguardi M, Biradar M, Makharia R (2012) Development of dispersed-catalyst/NSTF hybrid electrode. J Electrochem Soc F676–F682
66. Kongkanand A, Zhang J, Liu Z, Lai Y-H, Sinha P, Thompson EL, Makharia R (2014) Degradation of PEMFC observed on NSTF electrodes. J Electrochem Soc 161(6):F744–F753
67. Gierke TD, Munn GE, Wilson FC (1981) The morphology in Nafion perfluorinated membrane products, as determined by wide- and small- angle X-ray studies. J Polym Sci Polym Phys Ed 19(11):1687–1704
68. Schmidt-Rohr K, Chen Q (2008) Parallel cylindrical water nanochannels in Nafion fuel-cell membranes. Nat Mater 7(1):75–83
69. Kreuer K-D, Paddison SJ, Spohr E, Schuster M (2004) Transport in proton conductors for fuel-cell applications: simulations, elementary reactions, and phenomenology. Chem Rev 104(10):4637–4678
70. Kusoglu A, Weber AZ (2017) New insights into perfluorinated sulfonic-acid ionomers. Chem Rev 117(3):987
71. Dura JA, Murthi VS, Hartman M, Satija SK, Majkrzak CF (2009) Multilamellar interface structures in Nafion. Macromolecules 42(13):4769
72. Eastman SASA, Kim S, Page KAKA, Rowe BWBW, Kang S, Soles CLCL, Yager KGKG (2012) Effect of confinement on structure, water solubility, and water transport in Nafion thin films. Macromolecules 45(19):7920–7930
73. Modestino MA, Paul DK, Dishari S, Petrina SA, Allen FI, Hickner MA, Karan K, Segalman RA, Weber AZ (2013) Self-assembly and transport limitations in confined Nafion films. Macromolecules 46(3):867
74. Kusoglu A, Kushner D, Paul DKDK, Karan K, Hickner MAMA, Weber AZAZ (2014) Impact of substrate and processing on confinement of Nafion thin films. Adv Funct Mater 24(30):4763–4774
75. Bass M, Berman A, Singh A, Konovalov O, Freger V (2011) Surface-induced micelle orientation in Nafion films. Macromolecules 44(8):2893–2899
76. Kusoglu A, Dursch TJ, Weber AZ (2016) Nanostructure/swelling relationships of bulk and thin-film PFSA ionomers. Adv Funct Mater 26(27):4961
77. Page KA, Kusoglu A, Stafford CM, Kim S, Kline RJ, Weber AZ (2014) Confinement-driven increase in ionomer thin-film modulus. Nano Lett 14(5): 2299–2304
78. Ohira A, Kuroda S, Mohamed HFM, Tavernier B (2013) Effect of interface on surface morphology and proton conduction of polymer electrolyte thin films. Phys Chem Chem Phys 15(27):11494–11500
79. Kongkanand A (2011) Interfacial water transport measurements in Nafion thin films using a quartz-crystal microbalance. J Phys Chem C 115(22): 11318–11325
80. Siroma Z, Kakitsubo R, Fujiwara N, Ioroi T, Yamazaki SI, Yasuda K (2009) Depression of proton conductivity in recast Nafion film measured on flat substrate. J Power Sources 189(2):994–998
81. Mohamed HFM, Kuroda S, Kobayashi Y, Oshima N, Suzuki R, Ohira A (2013) Possible Presence of hydrophilic SO3H nanoclusters on the surface of dry ultrathin Nafion® films: a positron annihilation study. Phys Chem Chem Phys 15(5):1518–1525
82. Paul DK, Giorgi JB, Karan K (2013) Chemical and ionic conductivity degradation of ultra-thin ionomer film by X-ray beam exposure. J Electrochem Soc 160(4):F824
83. Paul DK, Karan K, Docoslis A, Giorgi JB, Pearce J (2013) Characteristics of self-assembled ultrathin Nafion films. Macromolecules 46(9):3461
84. Subbaraman R, Strmcnik D, Paulikas AP, Stamenkovic VR, Markovic NM (2010) Oxygen reduction reaction at three-phase interfaces. Chem Phys Chem 11(13):2825–2833
85. Kocha SS, Zack JW, Alia SM, Neyerlin KC, Pivovar BS (2012) Influence of ink composition on the electrochemical properties of Pt/C electrocatalysts. ECS Trans 50(2):1475–1485
86. Masuda T, Ikeda K, Uosaki K (2013) Potential-dependent adsorption/desorption behavior of perfluorosulfonated ionomer on a gold electrode surface studied by cyclic voltammetry, electrochemical quartz microbalance, and electrochemical atomic force microscopy. Langmuir 29(7):2420–2426
87. Kunimatsu K, Yoda T, Tryk DA, Uchida H, Watanabe M (2010) In situ ATR-FTIR study of oxygen reduction at the Pt/Nafion interface. Phys Chem Chem Phys 12(3):621–629
88. Ayato Y, Kunimatsu K, Osawa M, Okada T (2006) Study of Pt electrode/Nafion ionomer interface in HClO[sub 4] by in situ surface-enhanced FTIR spectroscopy. J Electrochem Soc 153(2):A203
89. Ono Y, Ohma A, Shinohara K, Fushinobu K (2013) Influence of equivalent weight of ionomer on local oxygen transport resistance in cathode catalyst layers. J Electrochem Soc 160(8):F779–F787
90. Kodama K, Shinohara A, Hasegawa N, Shinozaki K, Jinnouchi R, Suzuki T, Hatanaka T, Morimoto Y (2014) Catalyst poisoning property of sulfonimide acid ionomer on Pt (111) surface. J Electrochem Soc 161(5):F649–F652
91. Snyder J, Livi K, Erlebacher J (2013) Oxygen reduction reaction performance of [MTBD][beti]-encapsulated nanoporous NiPt alloy nanoparticles. Adv Funct Mater 23(44):5494–5501
92. Jomori S, Komatsubara K, Nonoyama N, Kato M, Yoshida T (2013) An experimental study of the effects of operational history on activity changes in a PEMFC. J Electrochem Soc 160(9):F1067–F1073

93. Liu H, Epting WK, Litster S (2015) Gas transport resistance in polymer electrolyte thin films on oxygen reduction reaction catalysts. Langmuir 31(36): 9853–9858
94. Jinnouchi R, Kudo K, Kitano N, Morimoto Y (2016) Molecular dynamics simulations on O2 permeation through Nafion ionomer on platinum surface. Electrochim Acta 188:767–776
95. Béléké AB, Miyatake K, Uchida H, Watanabe M (2007) Gas diffusion electrodes containing sulfonated polyether ionomers for PEFCs. Electrochim Acta 53(4):1972–1978
96. Omata T, Tanaka M, Miyatake K, Uchida M, Uchida H, Watanabe M (2012) Preparation and fuel cell performance of catalyst layers using sulfonated polyimide ionomers. ACS Appl Mater Interfaces 4(2):730–737
97. Dru D, Baranton S, Bigarré J, Buvat P, Coutanceau C (2016) Fluorine-free Pt nanocomposites for three-phase interfaces in fuel cell electrodes. ACS Catal 6(10):6993–7001
98. Park J-S, Krishnan P, Park S-H, Park G-G, Yang T-H, Lee W-Y, Kim C-SJ (2008) A study on fabrication of sulfonated poly(ether ether ketone)-based membrane-electrode assemblies for polymer electrolyte membrane fuel cells. J Power Sources 178(2):642–650
99. Yoon YJ, Kim T-H, Yu DM, Park J-Y, Hong YT (2012) Modification of hydrocarbon structure for polymer electrolyte membrane fuel cell binder application. Int J Hydrog Energy 37(18):13452–13461
100. Takami M (2013) Ionomers and ionoically conductive compositions for use as one or more electrode of a fuel cell
101. Fuel Cell Development Progress 2013 Report (n.d.). New Energy and Industrial Technology Development Organization (NEDO). http://www.nedo.go.jp/content/100575921.pdf
102. Kinoshita S, Tanuma T, Yamada K, Hommura S, Watakabe A, Saito S, Shimohira T (2014) Development of PFSA ionomers for the membrane and the electrodes. ECS Trans 64(3):371–375
103. Takahashi S, Mashio T, Horibe N, Akizuki K, Ohma A (2015) Analysis of the microstructure formation process and its influence on the performance of polymer electrolyte fuel-cell catalyst layers. Chem Electro Chem 2(10):1560–1567
104. Kim YS, Welch CF, Mack NH, Hjelm RP, Orler EB, Hawley ME, Lee KS, Yim S-D, Johnston CM (2014) Highly durable fuel cell electrodes based on ionomers dispersed in glycerol. Phys Chem Chem Phys 16(13):5927–5932
105. Amemiya, K.; Kobayashi, N.; Yoshida, T (2013) Fabrication process and its microscopic structure characteristics for high performance PEFC electrodes. In: Japanese society of automotive engineering. p 20135108
106. Adzic RR (2014) Contiguous platinum monolayer oxygen reduction electrocatalysts on high-stability-low-cost supports. Annual merit review DOE hydrogen and fuel cells and vehicle technologies programs. Washington, DC. https://www.hydrogen.energy.gov/pdfs/review14/fc009_adzic_2014_o.pdf
107. Steinbach A (2014) High performance, durable, low cost membrane electrode assemblies for transportation applications. Annual merit review DOE hydrogen and fuel cells and vehicle technologies programs. Washington, DC. https://www.hydrogen.energy.gov/pdfs/review14/fc104_steinbach_2014_o.pdf
108. Konno N, Mizuno S, Nakaji H, Ishikawa Y (2015) Development of compact and high-performance fuel cell stack. SAE Int J Altern Powertrains 4(1):2015-01–1175
109. Sasaki K, Naohara H, Choi Y, Cai Y, Chen W-F, Liu P, Adzic RR (2012) Highly stable Pt monolayer on PdAu nanoparticle electrocatalysts for the oxygen reduction reaction. Nat Commun 3:1115
110. Borup R, Meyers J, Pivovar B, Kim YS, Mukundan R, Garland N, Myers D, Wilson M, Garzon F, Wood D, Zelenay P, More K, Stroh K, Zawodzinski T, Boncella J, McGrath JE, Inaba M, Miyatake K, Hori M, Ota K, Ogumi Z, Miyata S, Nishikata A, Siroma Z, Uchimoto Y, Yasuda K, Kimijima K-I, Iwashita N (2007) Scientific aspects of polymer electrolyte fuel cell durability and degradation. Chem Rev 107(10):3904–3951
111. St-Pierre J, Zhai Y, Angelo MS (2014) Effect of selected airborne contaminants on PEMFC performance. J Electrochem Soc 161(3):F280
112. St-Pierre J, Zhai Y, Ge J (2016) Relationships between PEMFC cathode kinetic losses and contaminants' dipole moment and adsorption energy on Pt. J Electrochem Soc 163(3):F247
113. Teranishi K, Kawata K, Tsushima S, Hirai S (2006) Degradation mechanism of PEMFC under open circuit operation. Electrochem Solid-State Lett 9(10): A475
114. Ohma A, Yamamoto S, Shinohara K (2008) Membrane degradation mechanism during open-circuit voltage hold test. J Power Sources 182(1):39
115. Zhang J, Litteer BA, Coms FD, Makharia R (2012) Recoverable performance loss due to membrane chemical degradation in PEM fuel cells. J Electrochem Soc 159(7):F287
116. Okada T (1999) Theory for water management in membranes for polymer electrolyte fuel cells. Part 2. The effect of impurity ions at the cathode side on the membrane performances. J Electroanal Chem 465(1):18
117. Cai Y, Kongkanand A, Gu W, Moylan TE (2015) Effects of cobalt cation on low Pt-loaded PEM fuel cell performance. ECS Trans 69(17): 1047
118. Graedel TE, Allwood J, Birat J, Reck BK, Sibley SF, Sonnemann G, Buchert M, Hagelüken C (2011) Recycling rates of metals – a status report. A report of the Working Group on the Global Metal Flows to the International Resource Panel, United Nations Environment Programme, Paris

119. Hagelüken C (2012) Recycling the platinum group metals: a European perspective. Platin Met Rev 56(1):29–35

Books and Reviews

Gu W, Baker DR, Liu Y, Gasteiger HA (2009) Proton exchange membrane fuel cell (PEMFC) down-the-channel performance model. In: Vielstich W, Gasteiger HA, Lamm A, Yokokawa H (eds) Handbook of fuel cells: fundamentals, technology and applications. Wiley, Hoboken

Kongkanand A, Mathias MF (2016) The priority and challenge of high-power performance of low-platinum proton-exchange membrane fuel cells. J Phys Chem Lett 7(7):1127–1137

Kusoglu A, Weber AZ (2017) New insights into perfluorinated sulfonic-acid ionomers. Chem Rev 117(3):987

Weber AZ, Kusoglu A (2014) Unexplained transport resistances for low-loaded fuel-cell catalyst layers. J Mater Chem A 2(c):17207–17211

Zhang J (2013) PEM fuel cells and platinum-based electrocatalysts. In: Kreuer K-D (ed) Fuel cells: selected entries from the encyclopedia of sustainability science and technology. Springer, New York, pp 305–340